Angewandte Chemie
Eine Zeitschrift der Gesellschaft Deutscher Chemiker

Supporting Information

Concerted Rattling in $CsAg_5Te_3$ Leading to Ultralow Thermal Conductivity and High Thermoelectric Performance

Hua Lin[+], Gangjian Tan[+], Jin-Ni Shen, Shiqiang Hao, Li-Ming Wu, Nicholas Calta, Christos Malliakas, Si Wang, Ctirad Uher, Christopher Wolverton, and Mercouri G. Kanatzidis**

anie_201605015_sm_miscellaneous_information.pdf

Calculations details:

DFT calculations were carried out using the VASP[1] code with GGA-PBE[2] for the electronic exchange-correlation functional. The lattice thermal conductivity was calculated by using the Debye-Callaway formalism.[3–5] _ENREF_17This method has recently been shown to produce accurate values of lattice thermal conductivity, compared to experiment, for low-conductivity thermoelectric compounds. [4,6] The total lattice thermal conductivity could be written as a sum over one longitudinal κ_{LA} and two transverse κ_{TA} and $\kappa_{TA'}$ acoustic phonon branches: $\kappa_{Latt} = \kappa_{LA} + \kappa_{TA} + \kappa_{TA'}$. The partial conductivities κ_i (i corresponds to *TA*, *TA'* and *LA* modes) was given by

$$\kappa_i = \frac{1}{3} C_i T^3 \left\{ \int_0^{\Theta_i/T} \frac{\tau_c^i(x) x^4 e^x}{(e^x-1)^2} dx + \frac{\left[\int_0^{\Theta_i/T} \frac{\tau_c^i(x) x^4 e^x}{\tau_N^i (e^x-1)^2} dx\right]^2}{\int_0^{\Theta_i/T} \frac{\tau_c^i(x) x^4 e^x}{\tau_N^i \tau_U^i (e^x-1)^2} dx} \right\}$$

In this expression, Θ_i was the longitudinal (transverse) Debye temperature, $1/\tau_N^i$ was the scattering rate for normal phonon processes, $1/\tau_R^i$ was the sum of all resistive scattering processes, and $1/\tau_c^i = 1/\tau_N^i + 1/\tau_R^i$, $x = \hbar\omega/k_B T$, and $C_i = k_B^4/2\pi^2\hbar^3 v_i$, here, $\hbar$ was the Planck constant, k_B is the Boltzmann constant, ω was the phonon frequency, and v_i was the longitudinal or transverse acoustic phonon velocity.

The resistive scattering rate was the sum of scattering rates due to Umklapp phonon-phonon scattering ($1/\tau_U^i$), mass-difference impurity scattering ($1/\tau_m^i$), boundary scattering ($1/\tau_B^i$), and electron-phonon scattering ($1/\tau_{e-ph}^i$). In the pure single crystallize compound considered here, we ignored the effect of impurity scattering, and we assumed that boundary and electron-phonon scattering contributions could be ignored at temperatures above approximately 100 K. Thus the resistive scattering rate was mainly determined by the Umklapp phonon-phonon processes ($1/\tau_R^i \cong 1/\tau_U^i$). The normal phonon scattering and Umklapp could be written as,

$$\frac{1}{\tau_N^{LA}(x)} = \frac{k_B^5 \gamma_{LA}^2 V}{M\hbar^4 v_{LA}^5} x^2 T^5$$

$$\frac{1}{\tau_N^{TA/TA'}(x)} = \frac{k_B^5 \gamma_{TA/TA'}^2 V}{M\hbar^4 v_{TA/TA'}^5} x T^5$$

$$\frac{1}{\tau_U^i(x)} = \frac{k_B^2 \gamma_i^2}{M\hbar v_i^2 \Theta_i} x^2 T^3 e^{-\theta_i/3T}$$

where γ, V, and M were the Grüneisen parameter, the volume per atom, and the average mass of an atom in the crystal, respectively. The Grüneisen parameter could be defined as, $\gamma_i = -\frac{V\partial\omega_i}{\omega_i \partial V}$, characterizing the relationship between phonon frequency and volume change.

Low temperature thermal conductivity measurements:

Low temperature thermal conductivity measurements were carried out over the temperature range of 5–300 K using a longitudinal steady-state technique in a homemade cryostat. One end of a uniform bar-shaped sample was thermally anchored to the cold tip of a cryostat, which served as a heat sink. The other end was provided with a miniature strain gauge which served as the heat source. The power supplied to the heater is the product of the constant current passed through the resistive element of the strain gauge and the voltage developed across it. The thermal gradient set up along the length of the sample by the passage of heat from the heater was measured by a pair of fine calibrated copper-constantan thermocouples that were attached to the body of the sample with indium at two points along its length. Thermocouple leads were thermally anchored to the cold tip of the cryostat, the temperature of which was monitored by a calibrated Cernox thermometer establishing the absolute temperature. The Cu legs of the thermocouples also served to measure the potential difference. The sample is surrounded by two radiation shield to minimize radiation losses. The actual radiation loss measured at a room temperature is obtained by detaching the sample from the cold tip, letting the sample "hang" on its connecting leads and determining the heater power resulting in the identical average temperature of the sample as that during the normal thermal conductivity measurement. Thus specified radiation loss at 300 K was scaled to lower temperatures using the Stefan-Boltzmann law. [10,11]

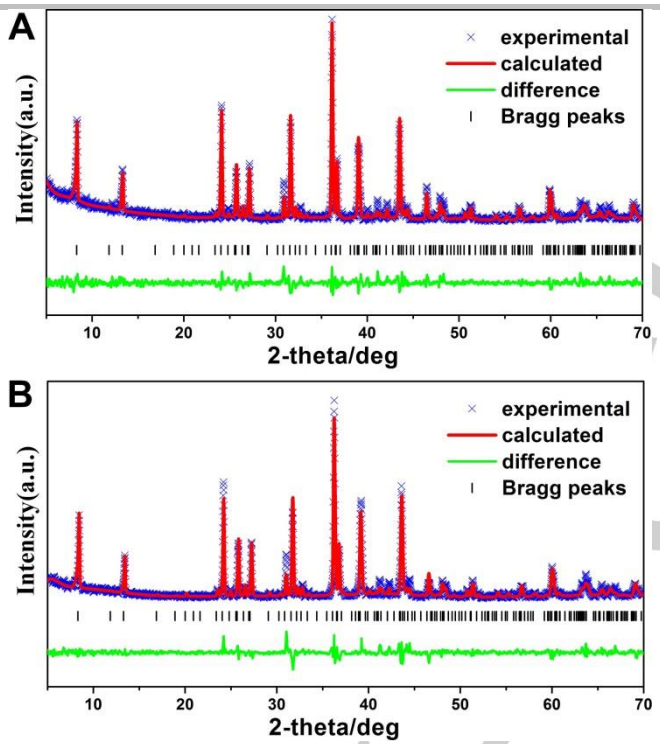

Figure S1. Experimental (black cross), calculated (red solid line), positions of the Bragg peaks (vertical bars) and difference (green) results of powder XRD refined by General Structure Analysis System (GSAS) for (**A**) as-synthesized and (**B**) SPSed polycrystalline $CsAg_5Te_3$.

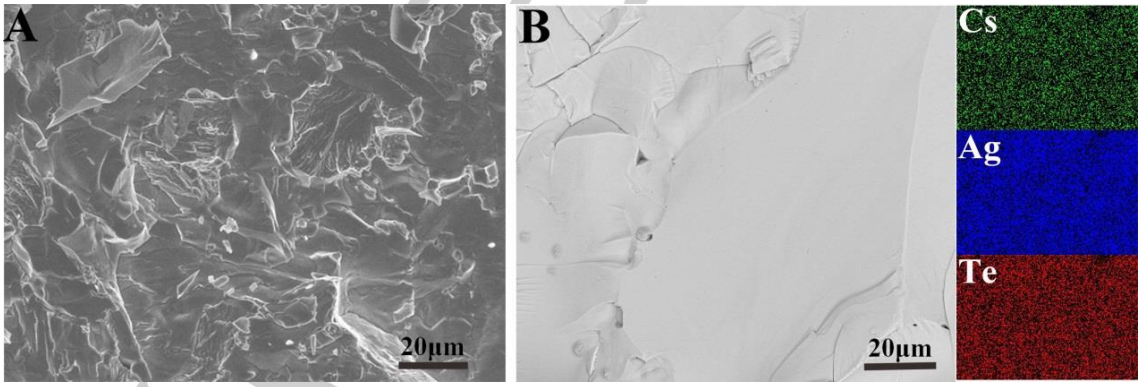

Figure S2. (A) The SEM image, and (B) the BSE image and the X-ray elemental mapping of Cs, Ag and Te elements of the freshly fractured surface obtained from the SPSed pellet of $CsAg_5Te_3$.

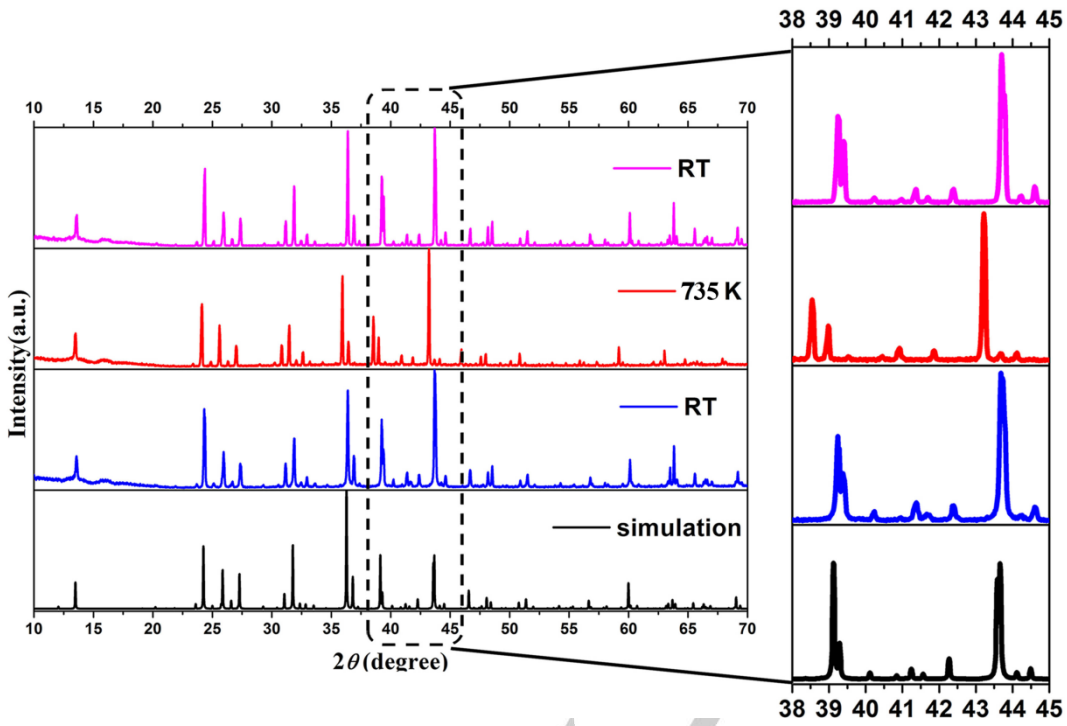

Figure S3. Temperature-dependent powder XRD patterns of the as-synthesized $CsAg_5Te_3$ collected between 300 and 735 K indicating the phase transition at ~730 K. The magnified part shows the variation of the major diffraction peaks indicating the phase transition.

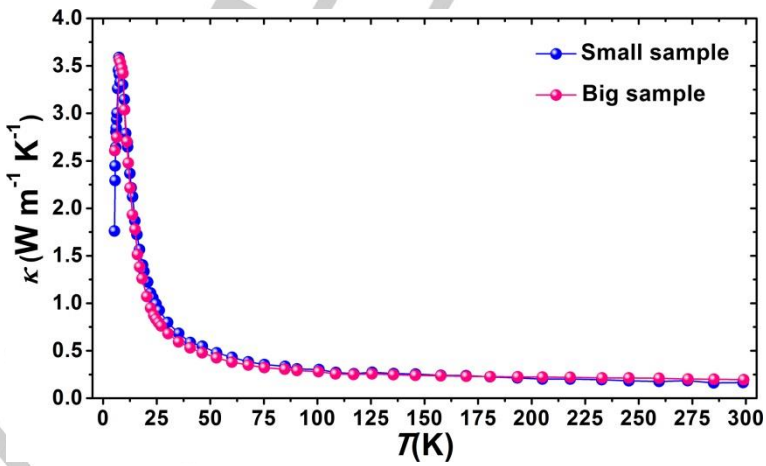

Figure S4. Low temperature thermal conductivities of $CsAg_5Te_3$ from 5 to 300 K.

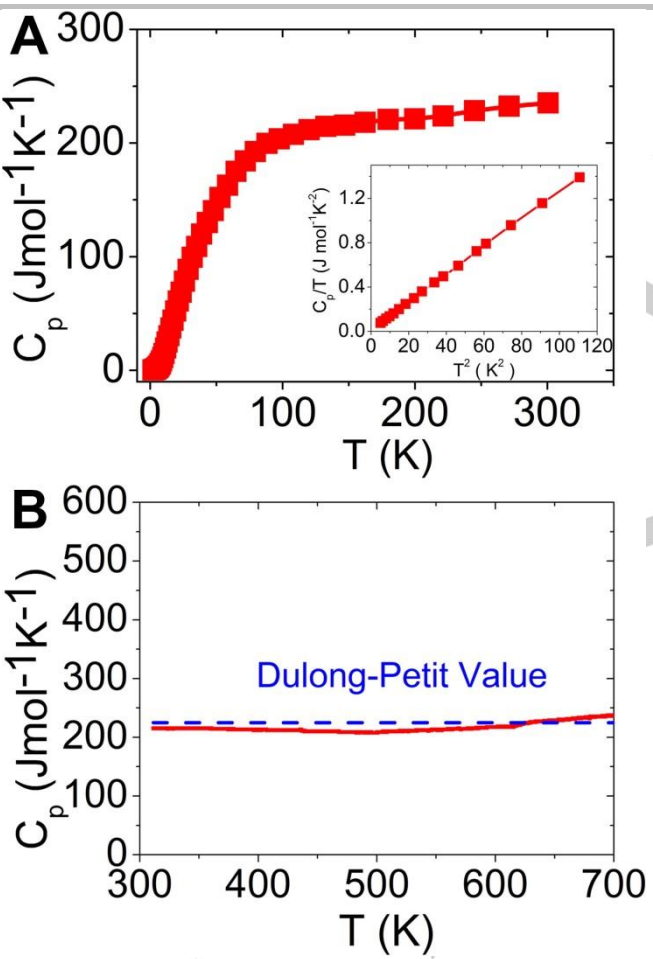

Figure S5. (**A**) The curve of C_p – Temperature (low temperature). Inset: The curve of C_p/T – T^2 at low temperature. (**B**) The curve of C_p-Temperature (RT to 700K).

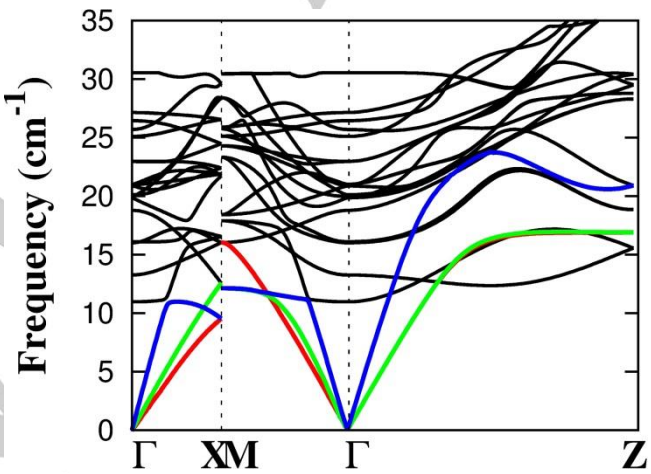

Figure S6. Phonon dispersion of $CsAg_5Te_3$ at the isotropically expanded volume $1.015V_0$.

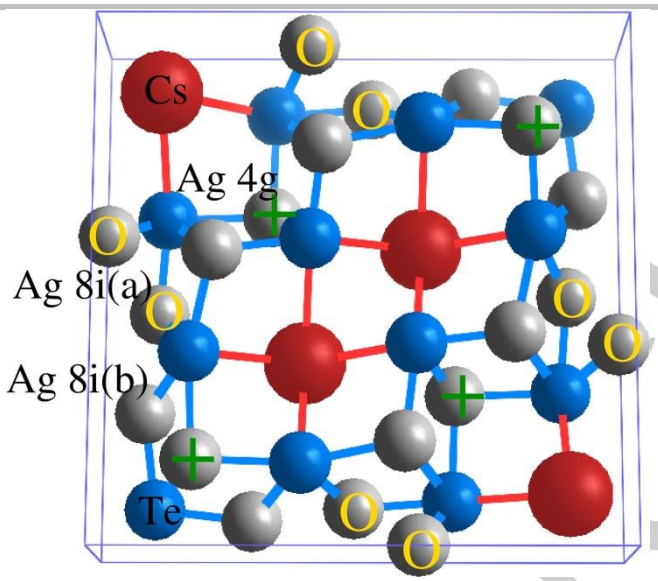

Figure S7. Atomic structure of $CsAg_5Te_3$ with Wyckoff sites. Ag3 atoms at the 4*g* site are silver balls labeled with green cross, Ag2 atoms at the 8*i*(a) site are silver balls marked with yellow circles, Ag1 atoms at the 8*i*(b) site are bare silver balls, big red spheres are Cs atoms and Te atoms are blue balls.

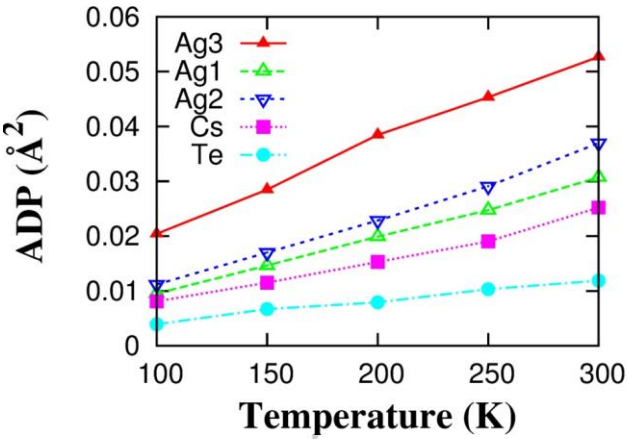

Figure S8. Temperature dependence of the ADP values from 100 to 300K.

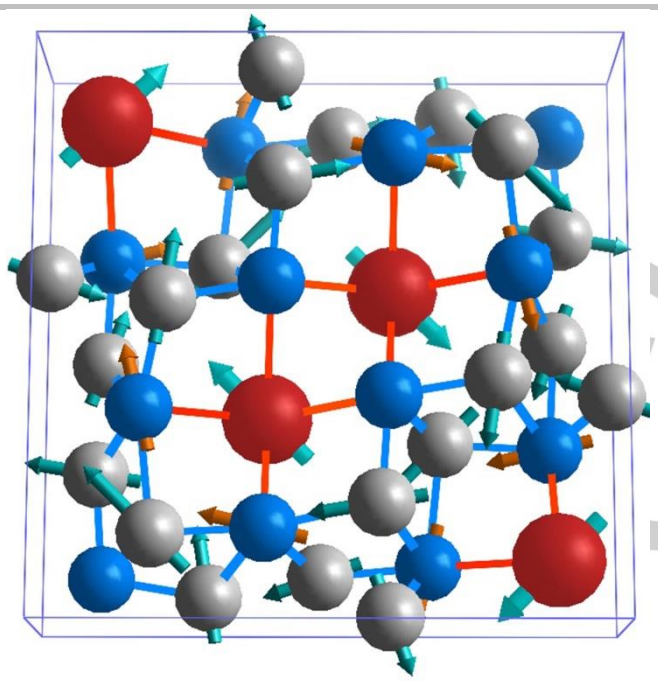

Figure S9. A snapshot of concerted rattling vibrational mode at Γ 14.6 cm^{-1}. The details of vibration mode can be seen from corresponding movie.

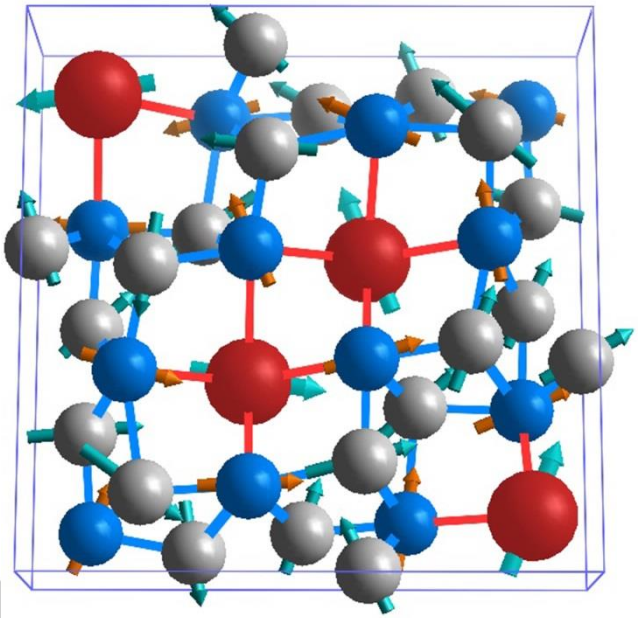

Figure S10. A snapshot of concerted rattling mode at 0.5(Γ+X) 13.2 cm^{-1}. The details of vibration mode can be seen from corresponding movie.

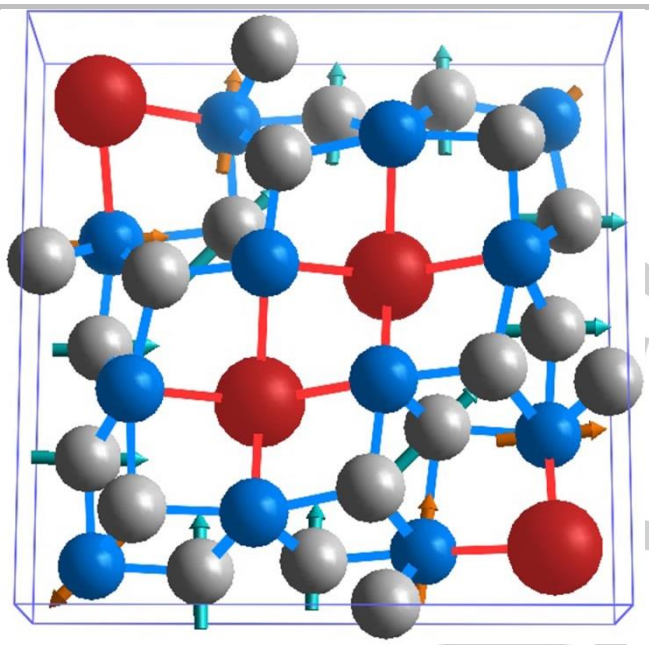

Figure S11. A snapshot of concerted rattling mode at Z 20.2 cm^{-1}. The details of vibration mode can be seen from corresponding movie.

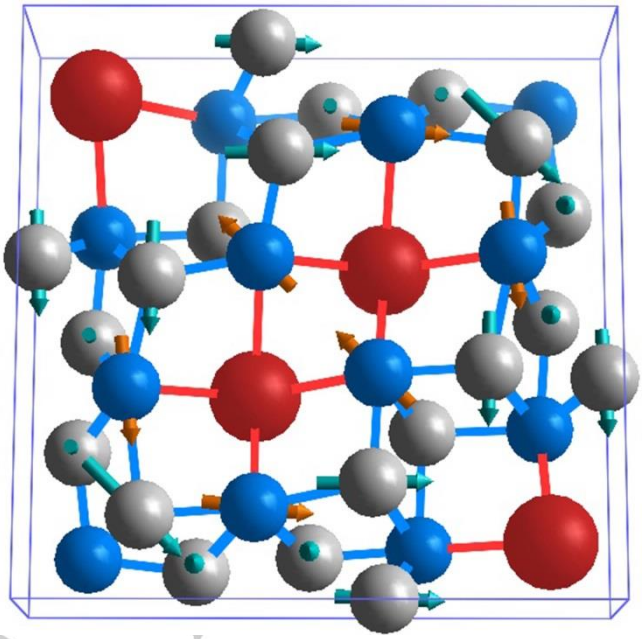

Figure S12. A snapshot of concerted rattling mode at Z 20.2 cm^{-1}. The details of vibration mode can be seen from corresponding movie.

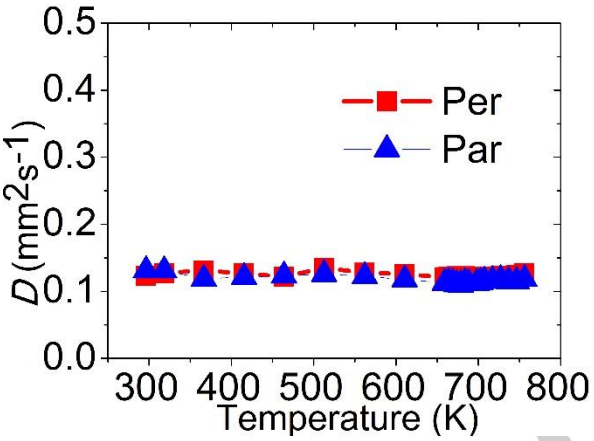

Figure S13. Thermal diffusivities of the SPSed polycrystalline $CsAg_5Te_3$ (Per: the perpendicular direction of SPS pressure, Par: the parallel direction of SPS pressure).

Table S1. Crystallographic Data and Refinement Details for $CsAg_5Te_3$ at room temperature (RT) and 100 K

Empirical formula	$CsAg_5Te_3$ (RT)	$CsAg_5Te_3$ (100 K)
Formula weight	1055.05	1055.05
Temperature(K)	293(2)	100(2)
Crystal system	Tetragonal	Tetragonal
Space group	*P4₂/mnm* (No.136)	*P4₂/mnm* (No.136)
Pearson code	*tP36*	*tP36*
a (Å)	14.645(2)	14.567(2)
c (Å)	4.5907(9)	4.5501(9)
V (Å^3)	984.6(3)	965.6(3)
Z	4	4
D_c (g·cm^{-3})	7.117	7.258
μ (mm^{-1})	22.043	22.478
Reflections collected/unique	14475/1233 [*R*(int) = 0.0893]	14142/1206 [*R*(int) = 0.1334]
GOOF on F^2	1.154	1.277
R_1, wR_2 ($I > 2\sigma(I)$) [a]	0.0508, 0.1111	0.0450, 0.1092
R_1, wR_2 (all data)	0.0555, 0.1135	0.0462, 0.1100
Largest diff. peak and hole (e· Å^{-3})	3.172, -2.823	2.606, -3.233

[a]: $R_1 = \Sigma||F_o| - |F_c||/\Sigma|F_o|$, $wR_2 = [\Sigma w(F_o^2 - F_c^2)^2/\Sigma w(F_o^2)^2]^{1/2}$

Table S2. Atomic Coordinates and Equivalent Isotropic Displacement Parameters of $CsAg_5Te_3$ at room temperature (RT) and 100 K.

RT					
Atom	Wyckoff site	*x*	*y*	*z*	U_{iso}(Å^2)
Te1	8*i*	0.61584(4)	0.17220(4)	0.0000	0.02079(17)
Te2	4*f*	0.40029(4)	0.40029(4)	0.0000	0.01979(18)
Cs1	4*f*	0.38666(5)	0.61334(5)	0.5000	0.0275(2)
Ag1	8*i*	0.41798(8)	0.21389(6)	0.0000	0.0402(2)
Ag2	8*i*	0.51770(6)	0.10450(6)	0.5000	0.0309(2)
Ag3	4*g*	0.32285(8)	0.32285(8)	0.5000	0.0445(4)
100 K					
Atom	Wyckoff site	*x*	*y*	*z*	U_{iso}(Å^2)
Te1	8*i*	0.61596(4)	0.17383(4)	0.0000	0.00998(15)
Te2	4*f*	0.40085(4)	0.40085(4)	0.0000	0.00975(18)
Cs1	4*f*	0.38733(4)	0.61267(4)	0.5000	0.01223(18)
Ag1	8*i*	0.41736(6)	0.21319(5)	0.0000	0.01562(18)
Ag2	8*i*	0.51670(5)	0.10401(5)	0.5000	0.01293(17)
Ag3	4*g*	0.32191(6)	0.32191(6)	0.5000	0.0169(2)

U_{eq} is defined as one third of the trace of the orthogonalized U_{ij} tensor.

Table S3. Anisotropic Displacement Parameters of $CsAg_5Te_3$ at room temperature (RT) and 100 K.

			RT			
Atom	U_{11}	U_{22}	U_{33}	U_{12}	U_{13}	U_{23}
Te1	0.0227(3)	0.0205(3)	0.0192(3)	0.00125(19)	0.00000	0.00000
Te2	0.0190(2)	0.0190(2)	0.0215(4)	0.0002(3)	0.00000	0.00000
Cs1	0.0280(3)	0.0280(3)	0.0266(4)	-0.0003(3)	0.00000	0.00000
Ag1	0.0496(6)	0.0226(4)	0.0483(6)	0.0023(3)	0.00000	0.00000
Ag2	0.0218(3)	0.0410(5)	0.0301(4)	-0.0035(3)	0.00000	0.00000
Ag3	0.0546(6)	0.0546(6)	0.0243(6)	-0.0120(7)	0.00000	0.00000
			100K			
Atom	U_{11}	U_{22}	U_{33}	U_{12}	U_{13}	U_{23}
Te1	0.0096(2)	0.0091(2)	0.0112(3)	0.00008(18)	0.00000	0.00000
Te2	0.0086(2)	0.0086(2)	0.0120(4)	0.0000(3)	0.00000	0.00000
Cs1	0.0115(2)	0.0115(2)	0.0137(4)	0.0000(2)	0.00000	0.00000
Ag1	0.0174(3)	0.0101(3)	0.0194(4)	0.0002(2)	0.00000	0.00000
Ag2	0.0094(3)	0.0151(3)	0.0143(3)	-0.0011(2)	0.00000	0.00000
Ag3	0.0187(3)	0.0187(3)	0.0133(4)	-0.0037(4)	0.00000	0.00000

Table S4. Effective band mass of $CsAg_5Te_3$ calculated for the top valence band (VBM) and the bottom conduction band (CBM) at the Γ-point.

	m^*/m_0 ($m_0 = 9.11\times10^{-31}$ kg)	
	VBM	CBM
Γ→X (*a* or *b* direction)	-3.53	0.30
Γ→Z (*c* direction)	-0.50	0.75

Table S5. Detailed calculated parameters in $CsAg_5Te_3$.

Parameters	Γ–X	M–Γ	Γ–Z
θ_{TA}(K)	14.8	24.5	29.3
$\theta_{TA'}$(K)	19.1	22.1	29.4
θ_{LA}(K)	19.1	30.6	35.9
υ_{TA}(m/s)	985.2	1243.6	1244.7
$\upsilon_{TA'}$(m/s)	1271.6	1491.4	1244.7
υ_{LA}(m/s)	2487.2	2301.1	2296.8
γ_{TA}	2.4	2.9	5.6
$\gamma_{TA'}$	2.9	4.2	5.6
γ_{LA}	5.9	5.8	3.8

Table S6. Percent weight and atomic composition of $CsAg_5Te_3$ at 10 randomly selected locations for EPMA analysis.

Location-1				Location-2			
Element	Weight%*	Atomic%*	Formula	Element	Weight%	Atomic%	Formula
Ag L	51.82	56.24	5.09	Ag L	51.18	55.61	4.97
Te L	36.16	33.17	3	Te L	36.54	33.56	3
Cs L	12.02	10.59	0.96	Cs L	12.28	10.83	0.97
Matrix	Correction	ZAF		Matrix	Correction	ZAF	
Location-3				Location-4			
Element	Weight%	Atomic%	Formula	Element	Weight%	Atomic%	Formula
Ag L	51.78	56.2	5.08	Ag L	51.77	56.19	5.06
Te L	36.17	33.19	3	Te L	36.33	33.33	3
Cs L	12.05	10.61	0.96	Cs L	11.9	10.48	0.94
Matrix	Correction	ZAF		Matrix	Correction	ZAF	
Location-5				Location-6			
Element	Weight%	Atomic%	Formula	Element	Weight%	Atomic%	Formula
Ag L	51.48	55.9	5.00	Ag L	51.61	56.03	5.06
Te L	36.53	33.53	3	Te L	36.18	33.2	3
Cs L	11.99	10.57	0.95	Cs L	12.22	10.77	0.97
Matrix	Correction	ZAF		Matrix	Correction	ZAF	
Location-7				Location-8			
Element	Weight%	Atomic%	Formula	Element	Weight%	Atomic%	Formula
Ag L	51.15	55.58	5.00	Ag L	51.02	55.46	4.99
Te L	36.28	33.33	3	Te L	36.31	33.36	3
Cs L	12.57	11.09	1.00	Cs L	12.67	11.18	1.01
Matrix	Correction	ZAF		Matrix	Correction	ZAF	
Location-9				Location-10			
Element	Weight%	Atomic%	Formula	Element	Weight%	Atomic%	Formula
Ag L	51.66	56.08	5.06	Ag L	51.19	55.62	5.02
Te L	36.25	33.27	3	Te L	36.22	33.27	3
Cs L	12.09	10.65	0.96	Cs L	12.59	11.1	1.00
Matrix	Correction	ZAF		Matrix	Correction	ZAF	
Average formula: $Cs_{0.98(2)}Ag_{5.03(3)}Te_3$ *All the numbers are normalized to 100%.							

References:

[1] G. Kresse, D. Joubert, *Phys. Rev. B* **1999**, *59***,** 1758.

[2] J. P. Perdew, K. Burke, M. Ernzerhof, *Phys. Rev. Lett.* **1996**, *77***,** 3865.

[3] M. Asen-Palmer, K. Bartkowski, E. Gmelin, M. Cardona, A. P. Zhernov, A. V. Inyushkin, A. Taldenkov, V. I. Ozhogin, K. M. Itoh, E. E. Haller, *Phys. Rev. B* **1997**, *56*, 9431.

[4] Y. Zhang, E. Skoug, J. Cain, V. Ozolins, D. Morelli, C. Wolverton, *Phys. Rev. B* **2012**, *85*, 054306.

[5] D. T. Morelli, J. P. Heremans, G. A. Slack, *Phys. Rev. B* **2002**, *66*, 195304.

[6] L. D. Zhao, S. H. Lo, Y. S. Zhang, H. Sun, G. J. Tan, C. Uher, C. Wolverton, V. P. Dravid, M. G. Kanatzidis, *Nature* **2014**, *508*, 373.

[7] B. Chen, J. H. Xu, C. Uher, D. T. Morelli, G. P. Meisner, J. P. Fleurial, T. Caillat, A. Borshchevsky, *Phys. Rev. B* **1997**, *55*, 1476.

[8] H. Chi, W. Liu, K. Sun, C. Uher, *Phys. Rev. B* **2013**, *88*, 045202.